



Electrospun poly(vinylidene fluoride)/poly(methyl methacrylate) grafted TiO₂ composite nanofibrous membrane as polymer electrolyte for lithium-ion batteries

Wei-Wei Cui ^{a,b}, Dong-Yan Tang ^{a,*}, Zai-Lin Gong ^a

^a Department of Chemistry, School of Science, Harbin Institute of Technology, Harbin 150001, China

^b College of Materials Science and Engineering, Harbin University of Science and Technology, Harbin 150040, China

HIGHLIGHTS

- PMMA-g-TiO₂ was synthesized by atom transfer radical polymerization (ATRP).
- PVdF/PMMA-g-TiO₂ composite nanofibrous membrane was fabricated by electrospinning method.
- PMMA-g-TiO₂ reduced the crystallinity and improved the electrolyte uptake of the membrane.
- The introduction of PMMA-g-TiO₂ enhanced the ionic conductivity and electrochemical stability.

ARTICLE INFO

Article history:

Received 19 June 2012

Received in revised form

24 August 2012

Accepted 14 September 2012

Available online 23 September 2012

Keywords:

Poly(methyl methacrylate) grafted titanium dioxide

Atom transfer radical polymerization

Poly(vinylidene fluoride)

Electrospinning

Polymer electrolyte

ABSTRACT

An organic/inorganic hybrid nanocomposite, poly(methyl methacrylate) grafted titanium dioxide (PMMA-g-TiO₂), is synthesized by atom transfer radical polymerization (ATRP). The hybrid nanocomposites are incorporated into poly(vinylidene fluoride) (PVdF) membranes during the electrospinning process to fabricate a composite nanofibrous membrane. Then the resultant fibrous polymer electrolyte is obtained by immersing the composite membrane into liquid electrolyte. FTIR, TEM, TGA, GPC, SEM, XRD, and DSC are used to characterize the structure, morphology and thermal properties of PMMA-g-TiO₂ hybrid nanocomposite and the composite nanofibrous membrane. The composite nanofibrous membrane is proven to be a good absorbent for the liquid electrolyte, and it exhibits a high electrolyte uptake and a high electrolyte retention ratio. The incorporation of PMMA-g-TiO₂ into the nanofibrous membrane inhibits the crystallization of PVdF during the solidification process and improves the ionic conductivity of the fibrous polymer electrolyte from 2.51×10^{-3} to 2.95×10^{-3} S cm⁻¹ at 20 °C. The electrochemical stability window of the polymer electrolyte is also enhanced due to the presence of PMMA-g-TiO₂.

© 2012 Elsevier B.V. All rights reserved.

1. Introduction

Poly(vinylidene fluoride) (PVdF) is a well-known semi-crystalline thermoplastic polymer with excellent film-forming ability and thermal stability [1]. Due to the high dielectric constant and strong chemical and electrochemical resistance, it has become a favorable polymer matrix for porous polymer electrolytes in lithium-ion batteries [2]. The porous polymer electrolytes based on PVdF can be prepared by different methods that include solution casting [3], phase inversion [4], and electrospinning. Among them, electrospinning is a predominant and promising technique to produce thin, flat and homogenous polymer membranes. In electrospinning

process, polymer melt or solution is forced through a spinneret by an electric field. The average diameter of the fibers produced by electrospinning is in the range of 100 nm–5 μm, and at least 10–100 times smaller than the conventional fibers produced by melt spinning [5]. Thus electrospun membranes exhibit high specific surface area and unique porous structures within the ranges of nano- to micro-meter.

As a semi-crystalline polymer, PVdF contains both an amorphous phase and a crystalline phase. The crystalline domains of PVdF hinder the penetration of liquid electrolytes and the migration of lithium ions, and hence the high-crystalline PVdF becomes one of the major factors to give the low ionic conductivity of polymer electrolytes [6]. Nevertheless, there remains the leakage of electrolyte solution due to a phase separation between this kind of polymer matrix and the absorbed electrolyte solution. The loss of electrolyte solution may further lead to a failing of the contact

* Corresponding author. Tel.: +86 451 86419643; fax: +86 451 86418270.

E-mail address: tangdongyang2011@yahoo.cn (D.-Y. Tang).

between electrode and electrolyte as well as a reduction of ionic conductivity. All these limit the use of electrospun PVdF membranes in lithium batteries [7]. For the purpose of tackling the aforementioned problems, several attempts have been carried out, which includes incorporating inorganic powders such as alumina, silica and titanium dioxide [8,9] or introducing other blending polymers like polyacrylonitrile (PAN), poly(methyl methacrylate)(PMMA), and thermoplastic polyurethane (TPU) into electrospun PVdF membranes [10–12]. In these systems, inorganic powders act as solid plasticizer [13], and blending polymers produce intermolecular interaction with PVdF [12], which hinder the reorganization of PVdF chains. All of these methods reduce the degree of crystallinity of PVdF in varying degree and improve the ionic conductivity of the polymer electrolytes.

Organic/inorganic hybrid nanocomposites typically consisted of polymer shells with incorporated inorganic cores are widely studied as potential materials in optical, electronic, magnetic, mechanical and catalytic fields [14]. As an effective way of preparing hybrid nanocomposites, atom transfer radical polymerization (ATRP) technique provides a good control over the thickness of grafted polymers and surface grafting density through the method of anchoring initiators to the surface of nanoparticles initially [15]. Wu et al. [16] fabricated hybrid silica nanoparticles grafted with thermoresponsive poly(*N*-isopropylacrylamide) (PNIPAM) brushes by means of ATRP and investigated their thermal phase transition behavior. Park et al. [17] synthesized $\text{TiO}_2/\text{Ag}/\text{poly}(\text{oxyethylene methacrylate})$ (POEM) ternary nanoparticles via ATRP for the application in photochromic switching. However, to the best of our knowledge, there are few reports on the fabrication of polymer electrolytes containing organic/inorganic hybrid nanocomposites up to now. In the present study, an organic/inorganic hybrid nanocomposite, PMMA grafted TiO_2 (PMMA-g- TiO_2), was synthesized by ATRP technique and then was electrospun together with PVdF to fabricate composite nanofibrous membrane. The corresponding fibrous polymer electrolyte was obtained by activating the electrospun membrane with the liquid electrolyte. TiO_2 was selected as inorganic core because it could contribute to the electrolyte dissociation by the Lewis acid–base interactions between the polar surface groups of TiO_2 and the electrolyte ionic species. PMMA was selected as polymeric shell because of its better compatibility with PVdF and its excellent affinity with carbonate-based liquid electrolyte, which would help the membranes entrap more liquid electrolyte and hinder the leakage of the electrolyte. PMMA-g- TiO_2 was expected to both exert the action of the polymer and retain partly the activity of inorganic particles. The structures of PMMA-g- TiO_2 were systematically examined, and the effects of PMMA-g- TiO_2 on the properties of the composite nanofibrous membrane and the fibrous polymer electrolyte were investigated.

2. Experimental

2.1. Materials

Titanium dioxide (TiO_2) nanoparticles were purchased from Hangzhou Wanjing New Material Co., Ltd. Methyl methacrylate (MMA) was purchased from Tianjin Bodi Chemical Co., Ltd. 3-Aminopropyltriethoxy silane (APTES) was purchased from Aladdin. 2-Bromoisobutyryl bromide, $\text{Cu}(\text{I})\text{Br}$, and pentamethyldiethylenetriamine (PMDETA) were purchased from Sigma–Aldrich. PVdF (KYNAR 761, ARKEMA) was purchased from Cmdic Xiamen Imp. & Exp. Co., Ltd. *N,N*-Dimethylformamide (DMF) and triethanolamine were in analytical reagent grade and were used as received. Liquid electrolyte (1 M LiPF_6 in ethylene carbonate (EC)/dimethyl carbonate (DMC) (1:1, wt/wt)) was supplied by Zhangjiagang Guotai–Huarong New Chemical Materials Co., Ltd.

2.2. Synthesis of PMMA-g- TiO_2 via ATRP method

1 g of TiO_2 nanoparticles and 0.1 mL of triethanolamine were dispersed in 50 mL of ethanol. Then 60 μL of aqueous ammonium solution and 0.94 mL of APTES were added to this dispersion after the dispersion was heated to 60 °C. The mixture was stirred using a magnetic bar at 50 °C for 12 h. Then, the mixture was purified through removing any unreacted silane coupling and ammonia by repeating centrifugal sedimentation and re-dispersion of the sediment in absolute ethanol for three times. The APTES modified TiO_2 (represented as TiO_2-NH_2) nanoparticles were obtained after being dried under vacuum. Then the obtained TiO_2-NH_2 nanoparticles, 50 mL of anhydrous toluene and 0.4 mL of pyridine were added into a 150 mL flask. 0.5 mL of 2-bromoisobutyryl bromide was added dropwise at 0 °C. The mixture was stirred for 0.5 h at 0 °C, followed by stirring at room temperature for 12 h. The resultant brominated TiO_2 nanoparticles (represented as TiO_2-Br) were obtained after repeating centrifugal sedimentation and re-dispersion of the sediment in absolute toluene.

300 mg of TiO_2-Br , 100 μL of PMDETA, 10 mL of MMA and 20 mL of DMF were placed into a Schlenk flask equipped with a magnetic stir bar and sealed with a rubber plug. The mixture were stirred and dispersed by ultrasonic for 0.5 h. After refrigeration in freezing brine for 0.5 h, the flask was evacuated and back-filled with N_2 gas for three times to remove any trace of oxygen. Then, the rubber plug was removed, and 0.09 g of CuBr was added into the flask under the protection flow of N_2 . The flask was immersed in a water bath at 60 °C immediately and kept stirring for 48 h. The final products were purified by repeating centrifugal sedimentation and re-dispersion of the sediment in acetone for three times to ensure the complete removal of the resultant homopolymers. PMMA-g- TiO_2 was obtained after further being dried at 60 °C under vacuum for 72 h.

2.3. Fabrication of PVdF/PMMA-g- TiO_2 composite fibrous polymer electrolytes

0.06 g of PMMA-g- TiO_2 was first dispersed into 4.72 g of DMF solvent by magnetic stirring under 60 °C. After 12 h, 1.0 g of PVdF was added into the solution, and the mixture was stirred for another 12 h. Then, the 18 wt% of PVdF mixed solution with PMMA-g- TiO_2 (6 wt% based on the weight of PVdF) was obtained. The mixed solution held in a 5 mL syringe was delivered into a stainless steel needle by a syringe pump (RWDLife Science RWD202, CN) with a flow rate of 0.003 mL min⁻¹. The needle was connected to an electrode of a high voltage supply, and a grounded aluminum foil was placed at 20 cm distance from the needle tip to collect the nanofibers membranes. The positive voltage applied to the needle was 14 kV. The environmental temperature was kept at 20 ± 2 °C, and the environmental humidity was kept at 15 ± 1%. For comparison, electrospun PVdF membrane without adding PMMA-g- TiO_2 was prepared. After electrospinning, all the membranes were dried in an oven at 80 °C for 72 h to remove the remaining solvent. Fibrous polymer electrolytes were obtained by soaking electrospun membranes into a liquid electrolyte of 1 M LiPF_6 in EC/DMC (1:1, wt/wt) for 12 h in a dry glove box.

2.4. Characterization

Fourier transform infrared (FTIR) spectra of pristine and grafted TiO_2 were obtained on a Nicolet AVATAR 360 system. Dried solids were pressed with KBr and the discs were scanned in the range of 4000–400 cm⁻¹ with a resolution of 2 cm⁻¹. Transmission electron microscopy (TEM) of PMMA-g- TiO_2 particles was performed using a Hitachi H-7650, with an acceleration voltage of 100 kV.

Thermogravimetric analysis (TGA) traces were obtained on a Perkin Elmer Pyris 6 thermogravimetric analyzer with a heating rate of $10\text{ }^{\circ}\text{C min}^{-1}$ over the temperature range at $30\text{--}750\text{ }^{\circ}\text{C}$ under the dry flow of N_2 at the rate of 20 mL min^{-1} . The molecular weight and molecular weight distribution were determined by a gel permeation chromatography (GPC) equipped with a $5\text{ }\mu\text{m}$ MIXED-C PL gel column (300×7.5 mm). Polystyrene was used as a calibration standard and tetrahydrofuran (THF) as the eluent with a flow rate of 1.00 mL min^{-1} . The injection apparatus was attached with a Refractive Index Detector (set at $30\text{ }^{\circ}\text{C}$) and in volume of $50\text{ }\mu\text{L}$. Scanning electron microscopy (SEM) images were obtained using an FEI Quanta 200 FEG scanning electron microscope. The samples were measured after sputtering a thin layer of Pt. The crystallinity of the electrospun membranes was measured on a Netzsch STA 449C differential scanning calorimeter (DSC) with a heating rate of $10\text{ }^{\circ}\text{C min}^{-1}$ over the temperature of $50\text{--}250\text{ }^{\circ}\text{C}$ under argon atmosphere. The wide-angle X-ray diffraction (WXRD) was carried on a Rigaku D/MAX-RB X-ray diffractometer recorded using $\text{Cu K}\alpha$ radiation with an experiment condition of 40 kV and 50 mA . The scan rate was $1\text{ }^{\circ}\text{ min}^{-1}$, and the sample was scanned in the range $5\text{--}80\text{ }^{\circ}$ with a step width of 0.02 ° . The wettability of the membranes was investigated by the liquid electrolyte contact angle measurement. The testing was measured by using a $2\text{ }\mu\text{L}$ liquid electrolyte droplet on the surface of the membranes under ambient conditions with a Powereach JC2000C optical contact angle meter. The images were captured in continuous shooting mode with interval of 20 p s^{-1} . The uptake of the liquid electrolyte was measured by soaking the electrospun membranes in the liquid electrolyte and weighing it at regular intervals after removing the excess liquid electrolyte by wiping it with tissue paper. The liquid electrolyte uptake was calculated using the following equation (Eq. (1)):

$$\varepsilon(\%) = \left(\frac{M - M_0}{M_0} \right) \times 100 \quad (1)$$

where ε is the uptake of the liquid electrolyte, M_0 is the mass of the membrane, and M is the mass of the membrane after being soaked in the liquid electrolyte. After being immersed in the electrolyte for 5 h , the leakage properties of the soaked polymer electrolytes which reached the equilibrium state were measured. The leakage of the electrolyte was calculated using the equation:

$$R(\%) = \frac{M_{\text{PE}}}{M_{\text{PE,saturated}}} \times 100 \quad (2)$$

where R is the relative absorption ratio of the liquid electrolyte, $M_{\text{PE,saturated}}$ is the mass of the polymer electrolyte when the membrane is fully saturated with the liquid electrolyte, and M_{PE} is the mass of the polymer electrolyte after a time interval when the saturated polymer electrolyte is squeezed by pressing between two pieces of filter paper. The ionic conductivities and electrochemical stability of polymer electrolytes were measured using electrochemical station (CHI 650D, USA). The ionic conductivities were measured by the AC impedance method in the frequency range of 0.01 Hz – 1 MHz . The sample was sandwiched between two stainless steel (SS) plates as blocking electrodes, and was kept at each measuring temperature for 30 min to ensure thermal equilibration of the sample at the temperature before measurement. Electrochemical stability was determined using linear sweep voltammetry with stainless steel (SS) as a working electrode and lithium as a reference electrode/counter electrode at the scan rate of 1 mV s^{-1} over the potential range of $0\text{--}6\text{ V}$ at room temperature.

3. Results and discussion

3.1. Synthesis and characterization of PMMA-g-TiO₂ via ATRP

FTIR measurement was used to confirm the successful synthesis of PMMA-g-TiO₂. Fig. 1 shows the FTIR spectra of pristine and grafted TiO₂. In the spectrum of pristine TiO₂ (Fig. 1a), the appearance of a strong peak at low frequencies (below 900 cm^{-1}) is due to the vibration absorbance from Ti–O/O–O bonds in TiO₂ lattice. In Fig. 1b, there appears a peak at 1130 cm^{-1} corresponding to the Si–O stretching frequency, which conforms the binding of ethoxy functional groups in 3-APTS to the free hydroxyl groups on TiO₂ surface to form a monolayer [18]. The FTIR spectrum of TiO₂–Br (Fig. 1c) demonstrates the characteristic absorption peaks occurring at 1654 cm^{-1} and 1535 cm^{-1} , which are ascribed to C=O bond and N–H bond stretching vibration of amide groups, respectively. Moreover, compared with pristine TiO₂ and TiO₂–NH₂, the absorption peak at low frequencies for TiO₂–Br obviously becomes broader, which is attributed to the overlapping of the absorption of C–Br groups (690 cm^{-1}) with the absorbance from Ti–O/O–O bonds [19]. This suggests the immobilization of 2-bromo isobutyryl groups onto the surface of TiO₂. Compare with the TiO₂–Br, the FTIR spectrum of PMMA-g-TiO₂ (Fig. 1d) shows several new adsorption peaks. The peak at 1735 cm^{-1} is assigned to the C=O bond stretching vibration of PMMA. The peaks at 2993 cm^{-1} and 2942 cm^{-1} are corresponding to C–H bond stretching vibrations of the CH₃ and CH₂ groups of grafted PMMA. The vibration absorption at 1481 cm^{-1} and 1147 cm^{-1} are attributed to the vibration of C–H bond and C–O bond, respectively. These indicate that PMMA is grafted successfully onto the surface of TiO₂ through ATRP reaction. Furthermore, the peak at 3429 cm^{-1} is assigned to the stretching vibration of hydroxyl groups, which suggests the residue of hydroxyl groups on the surface of TiO₂ after the grafting modification. The XPS spectra (see Supplementary materials for detail) further confirm that PMMA chains attach onto the surface of TiO₂ positively, and there is still the partial remaining surface hydroxyl after the surface modification.

Fig. 2 shows the TEM image of PMMA-g-TiO₂ particles. The gray area is attributed to the TiO₂ particles, and the light gray area is due to the grafted PMMA. It is shown that TiO₂ particles are encapsulated by PMMA shell, and the average shell thickness is around 6 nm thick. These characteristics from TEM further reveal that the

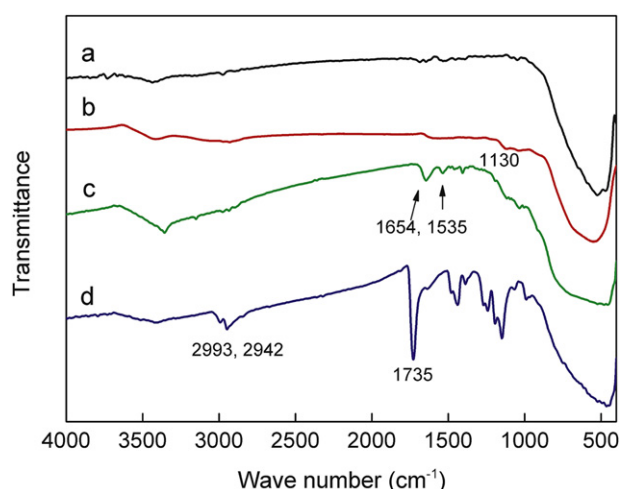


Fig. 1. FTIR spectra of (a) pristine TiO₂, (b) TiO₂–NH₂, (c) TiO₂–Br and (d) PMMA-g-TiO₂.

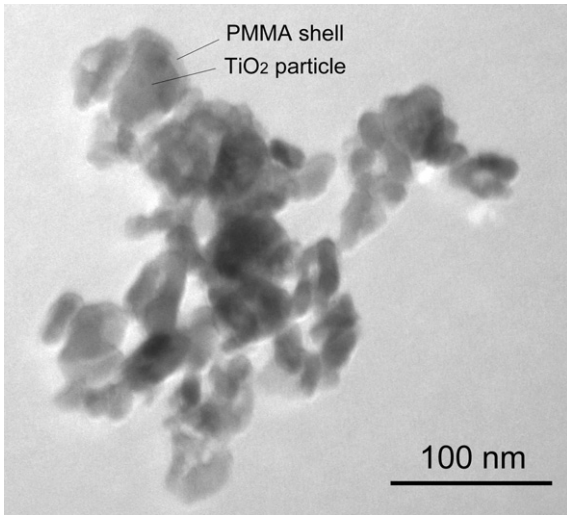


Fig. 2. TEM image of PMMA-g-TiO₂.

PMMA is grafted successfully on the surface of TiO₂ particles by ATRP method.

TGA method was used to determine the grafting ratio of 2-bromo isobutyryl groups and PMMA, and the results are shown in Fig. 3. The difference in weight loss between pristine TiO₂ and surface-grafted TiO₂ is ascribed to the amount of grafted organic content. As shown in Fig. 3a, pristine TiO₂ particles display a weight loss of 5.1 wt% up to 760 °C due to the loss of water molecules adsorbed onto the surface and the release of the structural water resulted from bonded hydroxyl groups. Compared with pristine TiO₂ particles, TiO₂–Br shows 7.8 wt% differences in the weight loss as shown in Fig. 3b. The thermogram of PMMA-g-TiO₂ (Fig. 3c) exhibits a major decomposition event at about 400 °C, which is due to the decomposition of grafted PMMA. The grafted PMMA content on TiO₂ surface estimated by the weight loss is nearly 38.7 wt%.

The length of the grafted polymer is a critical parameter for controlling and tuning the properties of the organic/inorganic nanocomposite. Gel permeation chromatography (GPC) was employed to determine the relative molecular weight (M_n) and molecular weight distribution (M_w/M_n) of PMMA grafted from the TiO₂ surface (The polymer was cleaved from the TiO₂ surface with hydrofluoric acid). From the GPC result shown in Fig. 4, it can be seen that the value of M_n is 12,540 g mol⁻¹ and M_w/M_n is 1.69. The

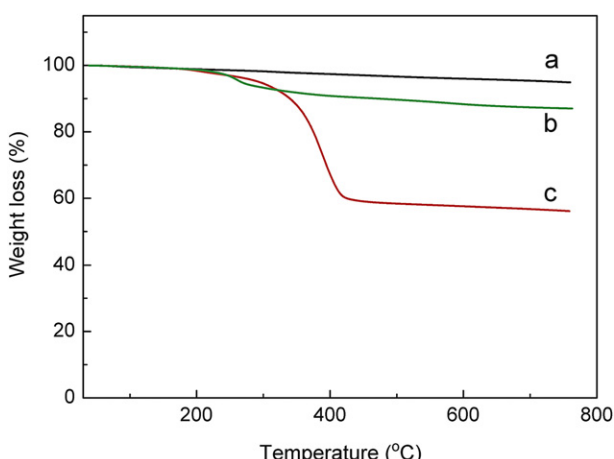


Fig. 3. TGA curves for (a) pristine TiO₂, (b) TiO₂–Br and (c) PMMA-g-TiO₂.

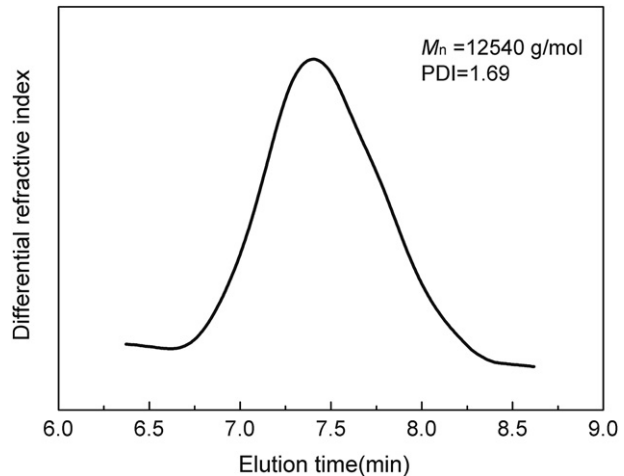


Fig. 4. GPC curve of grafted PMMA after the cleavage.

molecular weight distribution is unimodal and relative narrow, indicating that the ATRP process is performed in a controlled manner. The relatively low molecular weight facilitates the swelling of PMMA by the liquid electrolyte and helps to exert the action of PMMA and the residual hydroxyl groups on the surface of TiO₂.

3.2. Physical properties of electrospun PVdF/PMMA-g-TiO₂ composite nanofibrous membrane

Fig. 5 shows SEM images of electrospun PVdF and PVdF/PMMA-g-TiO₂ composite membranes. The fiber diameter histograms are also given in Fig. 5. It can be seen from SEM images that three-dimensional web structures are formed by the interconnected ultrafine fibers for both membranes, which indicate that the interstices are also fully interconnected. This unique porous structure is beneficial to entrap and retain electrolyte effectively, and it facilitates an electrolyte to diffuse smoothly into the cell assembly. The electrospun PVdF membrane has a uniform morphology with a mean fiber diameter of 0.336 μm. The electrospun PVdF/PMMA-g-TiO₂ composite membrane has similar mean diameters (0.333 μm), but the diameter distribution is broader than that of the electrospun PVdF membrane. For the two membranes, the electrospinning parameters which influence the diameter of fibers, such as applied voltage, feeding speed of polymer solution and tip-collector distance are all the same. So it is obvious that the introduction of PMMA-g-TiO₂ caused the increase of the viscosity of the polymer solution and led to the broader distribution of fiber diameter. Moreover, it is observed that several beads appear in the fiber structure after doping PMMA-g-TiO₂ particles. It is conceivable that the aggregation of the partial PMMA-g-TiO₂ particles causes the appearance of the beads.

Fig. 6 shows WXRD patterns of electrospun PVdF membrane and electrospun PVdF/PMMA-g-TiO₂ composite nanofibrous membrane. It is well established that PVdF can exhibit five different polymorphs (α , β , γ , δ and ϵ) depending on its processing conditions [20]. In this work, a very strong diffraction peak for PVdF membrane is observed at 2θ of 20.7°, which corresponds to 110 and 200 reflections of β phase. The weak diffraction peaks at 36.4° and 41.2° are related to 201 and 111 reflections of β phase, respectively [8]. A diffraction peak near 18.5° is assigned to 020 reflection α phase [21]. The results manifest the co-existence of α phase and β phase in the electrospun PVdF membrane, while the intensity of α phase peak is weaker significantly than that of β phase peak. This indicates the dominance of β phase in the electrospun membrane.

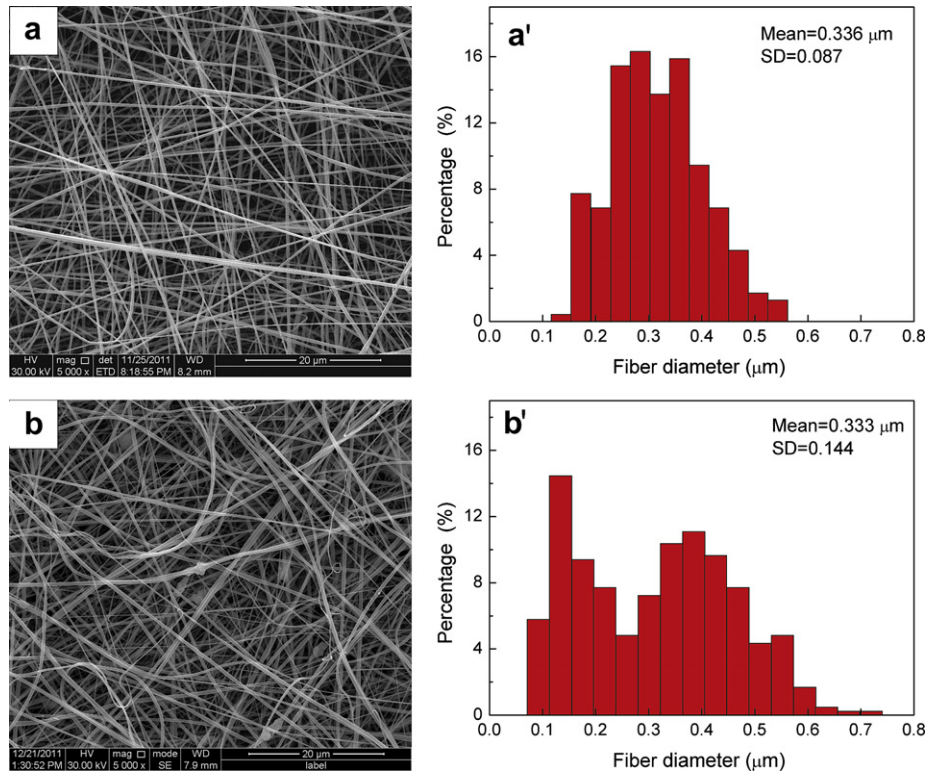


Fig. 5. SEM images (a, b) and corresponding fiber diameter distributions (a', b') of electrospun PVdF membrane (a, a') and electrospun PVdF/PMMA-g-TiO₂ composite nanofibrous membrane (b, b').

During electrospinning, polymer solution experiences two forces: One is shear force when it flows through a needle. The other one is Columbic force when the jet is elongated and accelerated by the high electric field applied. The combination of the two forces induces disentanglement and parallel packing of polymer chains and facilitates the orientation of the chains along the fiber axis. Hence, large numbers of β phase are formed. Compared with electrospun PVdF membrane, electrospun PVdF/PMMA-g-TiO₂ composite nanofibrous membrane shows new diffraction peaks at 2θ of 25.3° and 48.2°, which correspond to the characteristic peaks of TiO₂. This indicates the successful introduction of PMMA-g-TiO₂ into the electrospun membrane. Furthermore, the incorporations of

PMMA-g-TiO₂ into the electrospun membrane do not cause the position change of PVdF diffraction peaks, but the relative intensity of the peaks related to β phase (at 20.7°, 36.4° and 41.2°) to the peak related to α phase (at 18.5°) decreases clearly.

The difference of crystalline structure between electrospun PVdF membrane and electrospun PVdF/PMMA-g-TiO₂ composite nanofibrous membrane was also investigated by FTIR spectra, and the results are shown in Fig. 7. The spectra reveal that both membranes mainly contain β -phase crystal structure of PVdF. For electrospun PVdF membrane, the absorption peaks appearing at 472, 510, 842, and 1279 cm⁻¹ are identified to the characteristic

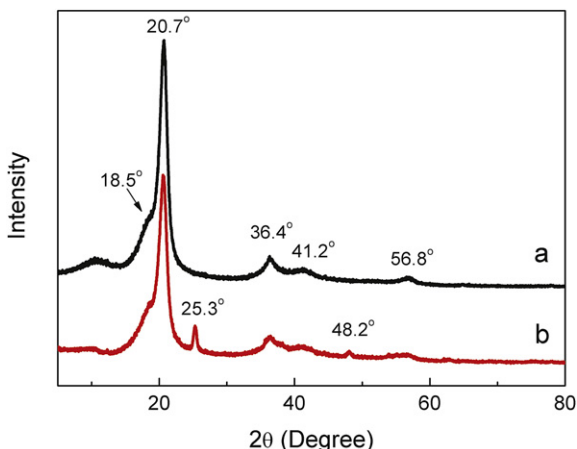


Fig. 6. WAXD patterns of (a) electrospun PVdF membrane and (b) electrospun PVdF/PMMA-g-TiO₂ composite nanofibrous membrane.

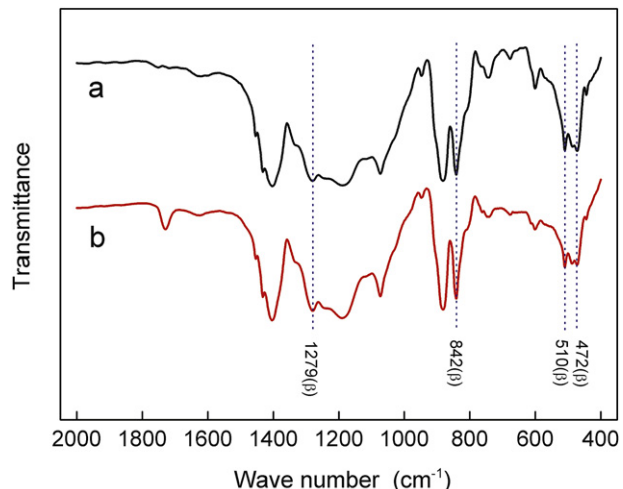


Fig. 7. FTIR spectra of (a) electrospun PVdF membrane and (b) electrospun PVdF/PMMA-g-TiO₂ composite nanofibrous membrane.

bands of β -phase for PVdF [22]. The band at 472 cm^{-1} is assigned to CF wagging vibration [23]. The 510 cm^{-1} band is assigned to CF_2 bending vibration [24]. The band at 842 cm^{-1} is assigned to CH_2 rocking vibration [25]. The band at 1279 cm^{-1} is assigned to CF_2 asymmetric stretching vibration [23]. These strong absorption peaks are the evidence of the high content of β -phase. In the case of PVdF/PMMA-g-TiO₂ composite nanofibrous membrane, a new absorption peak appears at 1728 cm^{-1} , which is related to C=O stretching vibration of PMMA. Furthermore, compared with the absorption peaks of electrospun PVdF membrane, the wider absorption peaks at $400\text{--}800\text{ cm}^{-1}$ of electrospun PVdF/PMMA-g-TiO₂ composite nanofibrous membrane are due to the overlap of Ti–O–Ti stretching vibration of TiO₂ with the absorption peaks. It also can be clearly observed that the absorption peaks related to β -phase crystal structure of PVdF decrease in intensity by introducing the PMMA-g-TiO₂. These results indicate that the orientation of the PVdF chains was inhibited by the PMMA-g-TiO₂ during the electrospinning process.

The effect of incorporation of PMMA-g-TiO₂ on the crystallinity of electrospun PVdF membrane was analyzed by measuring the melting heat during the crystal melting transition of PVdF using DSC. The DSC thermograms of electrospun membranes are shown in Fig. 8. The curves have similar shapes, and both exhibits an endothermic peak from 150 to $180\text{ }^\circ\text{C}$. The melting temperature (T_m) is noted as the temperature at the maximum value of the melting peak. It can be seen that the melting temperature of membranes are all at about $168\text{ }^\circ\text{C}$. The addition of PMMA-g-TiO₂ particles barely influences the melting temperature of membranes, while there is a considerable decrease of the melting enthalpy. The crystallinity (χ_c) can be calculated from the melting enthalpy from DSC curves by the following equation [26]:

$$\chi_c(\%) = \Delta H_f / \Delta H_f^* \times 100 \quad (3)$$

where ΔH_f^* is the crystalline melting enthalpy of perfectly crystalline PVdF (104.7 J g^{-1}) [27]. ΔH_f is the melting enthalpy of the electrospun membranes, which can be calculated from the integral area of the baseline and each melting curve. The crystallinity of the electrospun PVdF membrane is 40.54% . By incorporating PMMA-g-TiO₂, there is a considerable decrease of melting enthalpy, which corresponds to a crystallinity of 35.03% . This observation confirms that the addition of PMMA-g-TiO₂ inhibits the crystallization process of PVdF when it is drawn to form nanofibers. PMMA on the surface of TiO₂ particles has excellent compatibility with PVdF, and

the large groups ($\text{CH}_3\text{OCO}-$) in PMMA chain hinder the motion of polymer segments in crystallization [6]. Moreover, the hydrogen bond between the unreacted OH groups on the surface of TiO₂ and the fluorine in the PVdF chain may also partially contribute the hindrance of the motion of polymer segments [28]. The added filler decreases the degree of crystallization for fiber membrane and increases the amorphous regions of the polymer. The increase of amorphous regions is beneficial in achieving a higher ionic conductivity. Thus the results suggest that the PVdF/PMMA-g-TiO₂ composite fibrous polymer electrolytes may have an excellent ionic conductivity.

Fibrous polymer electrolytes were prepared by activating the electrospun membranes with the liquid electrolyte of 1 M LiPF_6 in EC/DMC (wt/wt). The wettability of the electrospun membranes was investigated by measuring the evolution of contact angles of the liquid electrolyte with time on the membranes (as shown in Fig. 9). The moment that the liquid electrolyte is dripped on the membrane is defined as the initial time. As shown in Fig. 9, after being dripped on the electrospun membranes, the drop of liquid electrolyte spreads quickly on the surface of both membranes, and penetrates into the interior of the membranes within 2 s . The quick penetration of the liquid electrolyte profits from the fully interconnected pore structure produced by electrospinning and the affinity between the polymer matrix and the liquid electrolyte.

The liquid electrolyte uptake behavior of the electrospun membranes is shown in Fig. 10. The uptake process is stabilized within 20 min . Both membranes exhibit a high electrolyte uptake. Electrospun PVdF membrane showed an electrolyte uptake of 310% after 300 min . For electrospun PVdF/PMMA-g-TiO₂ composite nanofibrous membrane, the uptake electrolyte is up to 360% after 300 min . The improved uptake capability is mainly due to the excellent affinity of PMMA-g-TiO₂ with carbonate-based liquid electrolyte and the increase of amorphous phase of PVdF [29]. A higher uptake of the liquid electrolyte means the existence of more Li^+ in the same volume, which leads to the high ionic conductivity of the composite polymer electrolyte.

It is a very important function for polymer electrolytes to prevent the leakage of electrolyte solution and ensure the stable properties of lithium batteries [9]. The loss of the electrolyte solution in the PVdF and PVdF/PMMA-g-TiO₂ fibrous polymer electrolytes are shown in Fig. 11. As shown in the figure, the relative absorption ratio (R) decreases gradually and approaches an equilibrium state until the leakage time reaches 120 min . The electrospun PVdF and the composite fibrous polymer electrolytes exhibit cumulative leakage about 21% and 16% of the initial absorption ratio, respectively. The composite membranes exhibited a less

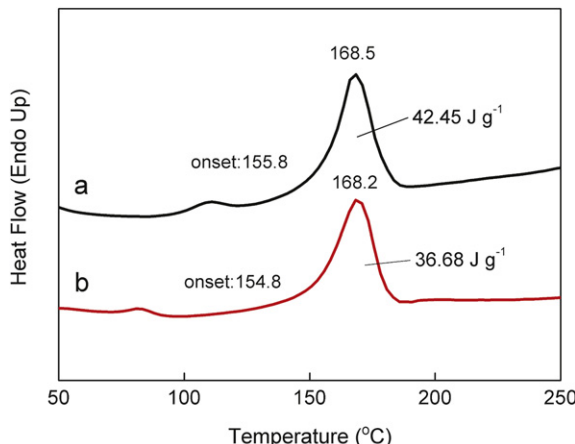


Fig. 8. DSC thermograms of (a) electrospun PVdF membrane and (b) electrospun PVdF/PMMA-g-TiO₂ composite nanofibrous membrane.

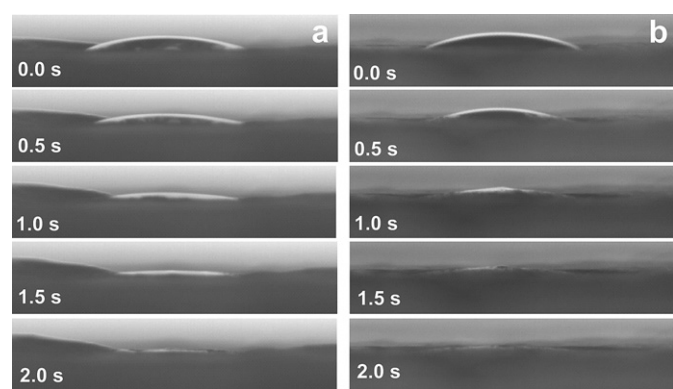


Fig. 9. The evolution of contact angles of the liquid electrolyte with time on (a) electrospun PVdF membrane and (b) electrospun PVdF/PMMA-g-TiO₂ composite nanofibrous membrane.

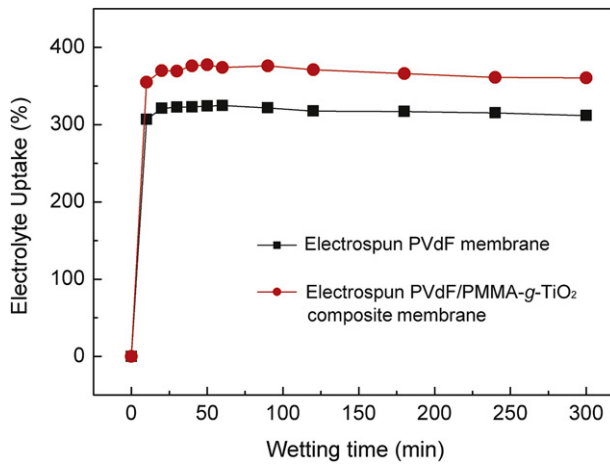


Fig. 10. Electrolyte uptake of the electrospun membranes (liquid electrolyte: 1 M LiPF₆ in EC/DMC (wt/wt)).

leakage than PVdF membrane. More amorphous phase of PVdF and the electrolyte affinity of PMMA might help to capture large amounts of liquid electrolytes.

3.3. Electrochemical properties of fibrous polymer electrolytes

The temperature dependence of ionic conductivities of polymer electrolytes over a temperature range of 20–70 °C is presented in Fig. 12. The ionic conductivities are all higher than 10^{-3} S cm⁻¹ and increase with the increase of temperature. The ionic conductivity at 20 °C is increased from 2.51×10^{-3} S cm⁻¹ to 2.95×10^{-3} S cm⁻¹ by introducing PMMA-g-TiO₂ into the electrospun membrane. PVdF fibrous polymer electrolytes are generally thought to comprise a solid fibrous phase, an amorphous swollen fibrous phase, and a liquid phase with the electrolyte solution in its pores [30]. Because the high crystalline content of PVdF prevents the migration of lithium ions, ion conduction mainly depends on the entrapped liquid phase in the pore structure. The high ionic conductivity can be mainly ascribed to the unique porous structure of the electrospun membranes. Furthermore, the amorphous swollen phase takes a tight hold of the electrolyte solution and prevents the solution's leakage. It also partially influences the ionic conductivity of the polymer electrolytes [31]. The increase of ionic conductivity by incorporation of PMMA-g-TiO₂ is due to the increase of the liquid electrolyte uptake and the amorphous phase content, which contributes to the formation of more tunnels allowing greater Li ion

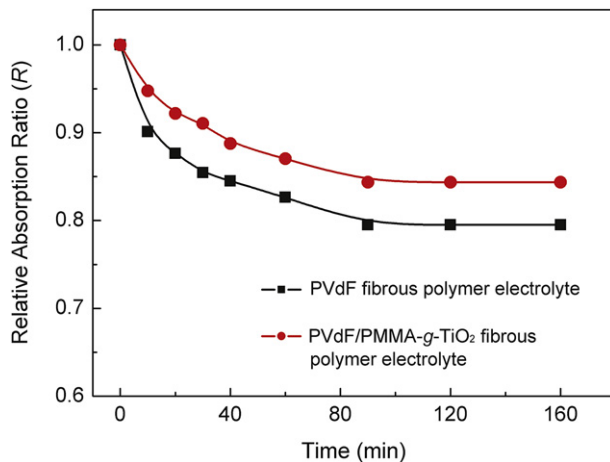


Fig. 11. Relative absorption ratio (R) of the fibrous polymer electrolytes.

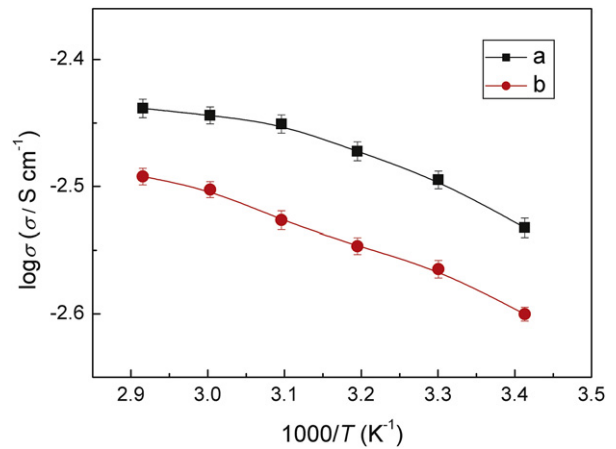


Fig. 12. Temperature dependence of ionic conductivity of (a) PVdF fibrous polymer electrolyte and (b) PVdF/PMMA-g-TiO₂ composite fibrous polymer electrolytes.

migration. Moreover, PMMA-g-TiO₂ in the amorphous phase can be swollen sufficiently by the carbonate-based liquid electrolyte. The liquid electrolyte thus would penetrate into PMMA shell and interact with the remaining surface hydroxyl of PMMA-g-TiO₂ by Lewis acid–base interactions, which might also partly contribute to the enhanced conductivities of the composite fibrous polymer electrolyte [28].

The results of electrochemical stability tests of the polymer electrolytes by linear sweep voltammetry are shown in Fig. 13. The linear sweep voltammetry was applied for a Li/polymer electrolyte/SS cell at room temperature. The current in the anodic high-voltage range results from a decomposition process associated with the electrolyte, and the onset voltage related to the increase of the current can be considered as the upper limit of the electrolyte stability range. In this work, both PVdF fibrous polymer electrolyte and PVdF/PMMA-g-TiO₂ composite fibrous polymer electrolytes exhibited good electrochemical stability. The onset voltage of current increase for PVdF fibrous polymer electrolyte is around 5.1 V. With the incorporation of the PMMA-g-TiO₂ into the polymer matrix, the voltage value for the onset of current increase is further increased up to 5.3 V. The higher electrochemical stability of composite fibrous polymer electrolytes than that of PVdF fibrous polymer electrolyte may be due to the combination of PVdF and PMMA-g-TiO₂. Due to the excellent affinity for PMMA-g-TiO₂, the electrolyte solution is more tightly trapped in the pores of the membrane in the composite

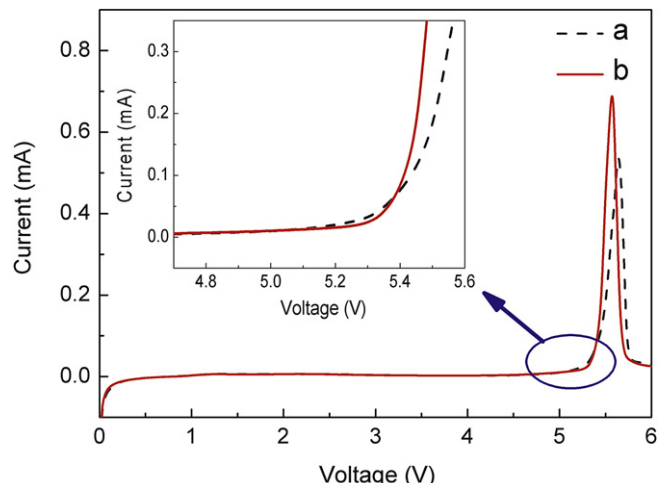


Fig. 13. Linear sweep voltammogram curves of (a) PVdF fibrous polymer electrolyte and (b) PVdF/PMMA-g-TiO₂ composite fibrous polymer electrolytes.

membrane. These results suggested that the prepared PVdF/PMMA-g-TiO₂ composite fibrous polymer electrolytes are expected to be suitable for application in lithium-ion batteries.

4. Conclusions

PMMA-g-TiO₂ was synthesized successfully via atom transfer radical polymerization. By electrospinning PVdF solution containing PMMA-g-TiO₂, PVdF/PMMA-g-TiO₂ composite fibrous membrane was prepared. The prepared membrane showed a porous morphology formed by interlayering of the fibers. The presence of PMMA-g-TiO₂ reduced the crystallinity of PVdF, and improved the electrolyte uptake and electrolyte retention ratio of electrospun membrane. Incorporation of PMMA-g-TiO₂ has been observed to be an effective method to improve the ionic conductivity and electrochemical stability of fibrous polymer electrolyte due to the increased amorphous content of PVdF and the excellent affinity between the liquid electrolyte and PMMA-g-TiO₂.

Acknowledgments

This work was supported by the Program for New Century Excellent Talents in University (NCET-08-0165).

Appendix A. Supplementary data

Supplementary data related to this article can be found at <http://dx.doi.org/10.1016/j.jpowsour.2012.09.049>.

References

- [1] F. Liu, N.A. Hashim, Y.T. Liu, M.R.M. Abed, K. Li, *J. Membr. Sci.* 375 (2011) 1.
- [2] A.M. Stephan, *Eur. Polym. J.* 42 (2006) 21.
- [3] Z.M. Li, J.G. Wei, F. Shan, J. Yang, X.L. Wang, *J. Polym. Sci. B: Polym. Phys.* 46 (2008) 751.
- [4] X.M. He, Q. Shi, X. Zhou, C.R. Wan, C.Y. Jiang, *Electrochim. Acta* 51 (2005) 1069.
- [5] D.H. Reneker, I. Chun, *Nanotechnology* 7 (1996) 216.
- [6] X.Y. Li, Q. Cao, X.Y. Wang, S.H. Jiang, H.Y. Deng, N. Wu, *J. Appl. Polym. Sci.* 122 (2011) 2616.
- [7] E.S. Choi, S.Y. Lee, *J. Mater. Chem.* 21 (2011) 14747.
- [8] Y.J. Kim, C.H. Ahn, M.B. Lee, M.S. Choi, *Mater. Chem. Phys.* 127 (2011) 137.
- [9] P. Raghavan, X.H. Zhao, J.K. Kim, J. Manuel, G.S. Chauhan, J.H. Ahn, C. Nah, *Electrochim. Acta* 54 (2008) 228.
- [10] A.I. Gopalan, P. Santhosh, K.M. Manesh, J.H. Nho, S.H. Kim, C.G. Hwang, K.P. Lee, *J. Membr. Sci.* 325 (2008) 683.
- [11] Z.Z. Zhao, J.Q. Li, X.Y. Yuan, X. Li, Y.Y. Zhang, J. Sheng, *J. Appl. Polym. Sci.* 97 (2005) 466.
- [12] N. Wu, Q. Cao, X.Y. Wang, Q.Q. Chen, *Solid State Ionics* 203 (2011) 42.
- [13] Z.H. Li, G.Y. Su, D.S. Gao, X.Y. Wang, X.P. Li, *Electrochim. Acta* 49 (2004) 4633.
- [14] W.P. Wang, H.M. Cao, G.J. Zhu, P. Wang, *J. Polym. Sci. A: Polym. Chem.* 48 (2010) 1782.
- [15] K. Matyjaszewski, P.J. Miller, N. Shukla, B. Immaraporn, A. Gelman, B.B. Luokala, T.M. Sclavon, G. Kickelbick, T. Vallant, H. Hoffmann, T. Pakula, *Macromolecules* 32 (1999) 8716.
- [16] T. Wu, Y.F. Zhang, X.F. Wang, S.Y. Liu, *Chem. Mater.* 20 (2008) 101.
- [17] J.T. Park, J.H. Koh, J.A. Seo, Y.S. Cho, J.H. Kim, *Appl. Surf. Sci.* 257 (2011) 8301.
- [18] G.K. Raghuraman, J. Ruhe, R. Dharmodharan, *J. Nanopart. Res.* 10 (2008) 415.
- [19] Y. Gao, X.P. Gao, Y.F. Zhou, D.Y. Yan, *Nanotechnology* 19 (2008).
- [20] J.F. Zheng, A.H. He, J.X. Li, C.C. Han, *Macromol. Rapid Commun.* 28 (2007) 2159.
- [21] W.A. Yee, S.X. Xiong, G.Q. Ding, C.A. Nguyen, P.S. Lee, J. Ma, M. Kotaki, Y. Liu, X.H. Lu, *Macromol. Rapid Commun.* 31 (2010) 1779.
- [22] S. Lanceros-Mendez, J.F. Mano, A.M. Costa, V.H. Schmidt, *J. Macromol. Sci. Phys.* B40 (2001) 517.
- [23] L.Z. Song, Z.J. Zhang, S.Z. Song, Z.M. Gao, *J. Mater. Sci. Technol.* 23 (2007) 55.
- [24] A. Salimi, A.A. Yousefi, *Polym. Test.* 22 (2003) 699.
- [25] D.S. Rana, D.K. Chaturvedi, J.K. Quamara, *J. Optoelectron. Adv. Mater.* 11 (2009) 705.
- [26] N. Wu, Q. Cao, X.Y. Wang, S. Li, X.Y. Li, H.Y. Deng, *J. Power Sources* 196 (2011) 9751.
- [27] K. Gao, X.G. Hu, C.S. Dai, T.F. Yi, *Mater. Sci. Eng. B* 131 (2006) 100.
- [28] Y.H. Ding, P. Zhang, Z.L. Long, Y. Jiang, F. Xu, W. Di, *Sci. Technol. Adv. Mater.* 9 (2008).
- [29] Y.H. Ding, P. Zhang, Z.L. Long, Y. Jiang, F. Xu, W. Di, *J. Membr. Sci.* 329 (2009) 56.
- [30] S.W. Choi, S.M. Jo, W.S. Lee, Y.R. Kim, *Adv. Mater.* 15 (2003) 2027.
- [31] J.R. Kim, S.W. Choi, S.M. Jo, W.S. Lee, B.C. Kim, *Electrochim. Acta* 50 (2004) 69.